Timothy G. McGee
Graduate Student

Justin W. Raade
Graduate Student

H. Kazerooni
Professor

Human Engineering and Robotics Laboratory,
Department of Mechanical Engineering,
University of California, Berkeley,
Berkeley, CA 94720

Monopropellant-Driven Free Piston Hydraulic Pump for Mobile Robotic Systems

The authors present a novel power supply for mobile robotic systems. A monopropellant (e.g., hydrogen peroxide) decomposes into high temperature gases, which drive a free piston hydraulic pump (FPHP). The elimination of fuel/oxidizer mixing allows the design of simple, lightweight systems capable of operation in oxygen free environments. A thermodynamic analysis has been performed, and an experimental FPHP has been built and tested. The prototype successfully pumped hydraulic fluid, although the flow rate was limited by the off-the-shelf components used. [DOI: 10.1115/1.1649972]

1 Introduction

The limitation of current power sources is one of the dominant bottlenecks preventing the more widespread appearance of fully autonomous field robotics. These robotic systems include any automated mobile platforms such as walking machines, robotic fish, or any similar system that must maintain energetic autonomy in non-laboratory environments. To overcome the power supply problem in past research efforts, researchers have typically either used a large number of batteries to demonstrate the system performance for a short time in the field, or they used an umbilical cord to power their system from a large stationary power supply. Thus, in order to achieve true energetic autonomy for many mobile robotic systems, new advances in power source technology are still required.

Most human scale and smaller robotic systems have power requirements ranging from 10 W to 2,000 W. The dominant traditional power supplies in this range are electric batteries, fuel cells, and small internal combustion (IC) engines, such as model airplane engines. These power supplies have significant drawbacks, however. The low energy density of batteries prevents them from being applicable for any prolonged period of time. Although fuel cells do have larger energy density than batteries, they lack high power density and cannot create bursts of power quickly. Electric actuators are also much larger and bulkier than hydraulic or pneumatic actuators for comparable power outputs. While the high energy density of gasoline is desirable, all hydrocarbon engines require elaborate systems for air compression and ignition in addition to many moving parts such as crank shafts and pistons. Small IC engines must also run at extremely high speeds in order to achieve good power densities. Thus, gear reduction systems are required to connect these engines to pumps, adding complexity to the system. Hydrocarbon engines are also limited by their dependence on the oxygen in air, restricting underwater and space applications.

Given these limitations of more traditional power sources, the use of monopropellant technology for mobile robotic power supplies has promising potential. Monopropellants refer to a class of energetic liquids, such as high concentration hydrogen peroxide and hydrazine, which decompose upon contacting a solid catalyst surface and release heat:

$$\text{Monopropellant} + \text{catalyst} \rightarrow \text{gas products} + \text{heat} \qquad (1)$$

The energy produced by this reaction can be harnessed by allowing the expanding hot gases to perform work on a piston or turbine, just as the combustion products of an IC engine are used to perform work. Since the monopropellant reaction does not require an oxidizer, fuel/oxidizer mixing is eliminated. This allows the design of simple, lightweight systems with increased power and energy densities, and operation in oxygen free environments, such as underwater or space. Unlike IC engines, monopropellant driven engines do not require a compression stage. This eliminates idling when there is no load on the system, and allows a monopropellant power supply to produce power on demand by producing discrete engine strokes. The ability to control individual strokes of the engine also provides more flexibility for the overall control strategy for the power supply. Furthermore, hydrogen peroxide, one of the available monopropellants, decomposes into steam and oxygen, which are nontoxic to humans.

Monopropellants have a successful history of applications. They have most often been used as a rocket propellant in spacecraft including the Mercury spacecraft, satellite attitude control, and an experimental Personal Rocket Belt [1]. Monopropellants have also been successfully used to power turbine driven hydraulic pumps for the X-15 Rocket Plane [2] and NASA Space Shuttle [3]. While no literature was found on a detailed study of the use of monopropellants for small scaled robotics applications outside of the recent past, a NASA sponsored technology study from 1967 mentions the possibility of using the hot gas from monopropellant decomposition to power human scaled robotics [4]. More recently, there have been some renewed investigations into the development of monopropellant power supplies. Amendola and Petillo outline the benefits of using various monopropellants, including hydrogen peroxide, to drive a piston engine in their 2001 patent [5]. Also, a team from Vanderbilt University has recently done some extensive testing using decomposed hydrogen peroxide to directly power hot gas cylinders [6].

The two main approaches for monopropellant robotic power supplies are to use the decomposed hot gases to directly power actuators or to power a hydraulic system [4]. Although a monopropellant driven hydraulic system is bulkier and less efficient than a system which directly uses the decomposed hot gases, it does provide several advantages, which could make it more desirable for certain applications. Since hydraulic fluid is far less compressible than the hot gas, higher bandwidth actuation can be achieved. The higher pressures that can be obtained in hydraulic fluid, when compared to compressed gas, also allow the use of smaller actuators to achieve the same forces. A centralized hydraulic pump also contains the hot decomposition gases to a single location where they can be vented using passive exhaust ports. Thus it does not require the development of control valves that can withstand the high decomposition temperatures of the monopropellants.

Contributed by the Dynamic Systems, Measurement, and Control Division of THE AMERICAN SOCIETY OF MECHANICAL ENGINEERS for publication in the ASME JOURNAL OF DYNAMIC SYSTEMS, MEASUREMENT, AND CONTROL. Manuscript received by the ASME Dynamic Systems and Control Division March 5, 2003; final revision, July 8, 2003. Associate Editor: N. Manring.

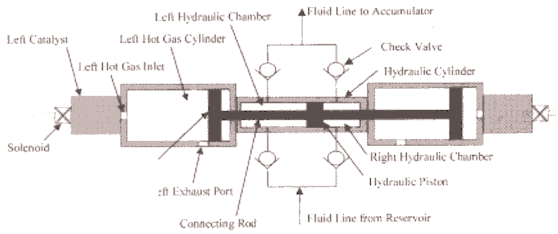

Fig. 1 Monopropellant FPHP

This paper investigates a hydraulic system which uses hydrogen peroxide to drive a novel free piston hydraulic pump (FPHP). The FPHP combines two past areas of research: the use of monopropellants to power hydraulic systems with turbine driven pumps [2,3] and free piston hydraulic pumps driven by IC engines [7–12]. Although gasoline and other hydrocarbon fuels have very high energy densities, a breakthrough in the development of a reliable IC free piston engine hasn't occurred, primarily resulting from several technical challenges that include maintaining a constant compression ratio with the absence of a crank shaft, properly timing the ignition, and starting the engine. These challenges arise from the need to compress the air-fuel mixture in IC engines and to ignite the mixture at a certain piston location. Since monopropellants systems do not require compression, these problems are eliminated.

2 Description of FPHP

The basic power source design, illustrated in Fig. 1, consists of two *Hot Gas Cylinders* and a *Hydraulic Cylinder*. A cycle of the FPHP operation begins with the opening of the *Left Solenoid Valve*, allowing liquid monopropellant to flow into the *Left Catalyst Bed*. The *Catalyst Bed*, typically a metallic mesh, decomposes the liquid monopropellant into high pressure decomposition gases, which enter the *Left Hot Gas Cylinder* through the *Left Hot Gas Inlet* (Fig. 2a). The expanding hot gas performs work on the *Left Hot Gas Piston*, forcing it to the right. Since the *Hot Gas Pistons* are rigidly connected to the *Hydraulic Piston* by a *Connecting Rod*, forming a single free piston assembly (FPA), the *Hydraulic Piston* is also forced to the right. This motion drives the hydraulic fluid in the *Right Hydraulic Chamber* through a *Check Valve* and into an accumulator, and draws low pressure hydraulic fluid from a reservoir into the *Left Hydraulic Chamber* (Fig. 2b). When the piston reaches the end of its stroke, the gases are vented to the atmosphere through the *Left Exhaust Port*, which is machined into the cylinder (Fig. 2c). This marks the end of the first stroke of one cycle. During the second stroke, monopropellant is injected into the *Right Catalyst Bed*, resulting in hot gas expansion in the *Right Hot Gas Cylinder*, which drives the piston to the left. This forces the hydraulic fluid in the *Left Hydraulic Chamber* into the high pressure accumulator, and draws in more low pressure fluid into the *Right Hydraulic Chamber*. This cycle is then repeated. Thus, the FPHP is able to produce power with each stroke, since the *Check Valves* ensure that the hydraulic fluid is drawn into each *Hydraulic Chamber* when the piston moves in one direction, and pumped out at high pressure when the piston returns in the other direction. Since the area of the hydraulic piston is smaller than the hot gas piston, pressure amplification is produced. This allows the FPHP to achieve higher pressures in the hydraulic fluid.

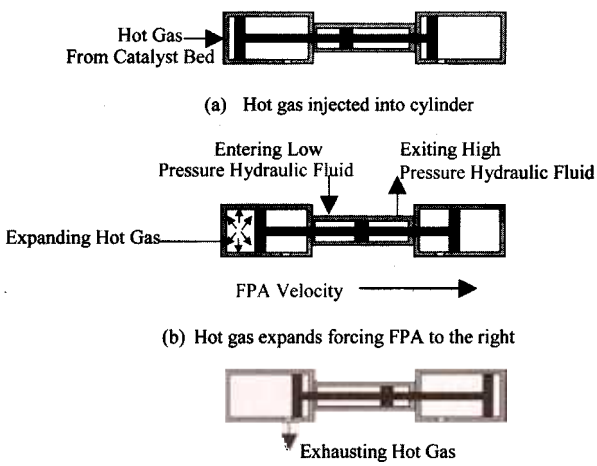

(a) Hot gas injected into cylinder

(b) Hot gas expands forcing FPA to the right

(c) Hot gas vents through exhaust port

Fig. 2 Operation of Free Piston Hydraulic Pump

Table 1 Comparison of Various H_2O_2 Concentrations

Concentration	Energy Density	Decomposition Temperature

The design of this engine is much simpler than existing IC engines. There are no cams, complex exhaust port routing, or fuel mixture requirements. There is only one basic moving part: the FPA. This simple design results in a compact, reliable, and robust machine. Another important feature of this system is that as a result of the simple radial geometry it can be manufactured fairly inexpensively.

3 H_2O_2 as a Monopropellant

Although the FPHP could make use of any monopropellant, hydrogen peroxide was chosen for the prototype. Hydrazine, the most widespread monopropellant in the aerospace community because of its high energy density, is carcinogenic and very costly to handle. Hydrogen peroxide, on the other hand, has several characteristics making it much safer to use. First, it has a very low vapor pressure allowing personnel to handle the monopropellant without respirator systems. Furthermore, by diluting high strength peroxide with water, any immediate dangers can be easily eliminated. Finally, the decomposition products of hydrogen peroxide are hot steam and oxygen, which are nontoxic to humans. In addition to these benefits, since there is a relatively large market for high concentration hydrogen peroxide in the textile and integrated circuit industries, there is an infrastructure in place to commercially obtain the monopropellant. These advantages make hydrogen peroxide the best choice to study the FPHP in a laboratory environment.

One hundred percent hydrogen peroxide reacts according to the following reaction:

$$2H_2O_2(l) \xrightarrow{\text{catalytic surface}} 2H_2O(g)+O_2(g)+1.6\text{MJ/kg} \quad (2)$$

Although pure hydrogen peroxide is desirable from an energy density standpoint, lower concentration 70% hydrogen peroxide with 30% water and 90% hydrogen peroxide with 10% water are less expensive and readily available for testing. The vaporization of the extra water in these lower concentration monopropellants further reduces the energy density, however. Table 1 outlines the

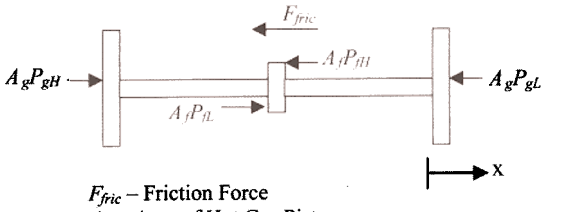

F_{fric} – Friction Force
A_g – Area of Hot Gas Piston
A_f – Area of Hydraulic Fluid Piston
P_{gH} – Hot Gas Pressure on High Pressure Side
P_{gL} – Hot Gas Pressure on Low Pressure Side
P_{fH} – Hydraulic Fluid Pressure on High Pressure Side
P_{fL} – Hydraulic Fluid Pressure on Low Pressure Side

Fig. 3 Free Body Diagram of FPA

monopropellant energy densities, and decomposition temperatures for various concentrations of hydrogen peroxide.

4 Dynamic Analysis of FPHP

4.1 Theoretical Modeling. The dynamics of the FPHP are determined by the dynamics of the free piston assembly motion which are governed by:

$$\Sigma F = m\ddot{x} = A_g(P_{gH} - P_{gL}) - A_f(P_{fH} - P_{fL}) - F_{fric} \quad (3)$$

where m denotes the mass of the FPA, $\ddot{x}$ is its linear acceleration and ΣF is the sum of the forces acting on the FPA, which are illustrated in Fig. 3. No force is modeled on the back faces of the hot gas pistons since both are well vented to atmosphere.

The hot gas cylinder of the FPHP is modeled as a control volume with the hot gases entering at the adiabatic decomposition temperature (T_{ad}) of the hydrogen peroxide as illustrated in Fig. 4. Since each stroke occurs in a relatively short time, very little heat is lost through the cylinder walls. The process is therefore assumed to be adiabatic. The energy balance for an adiabatic control volume with entering gas is:

$$\dot{m}_i h_i - \dot{W} = \frac{d}{dt} E_{system} \quad (4)$$

where $\dot{m}_i$ is the mass flow rate of hot gas into the control volume, h_i is specific enthalpy of the gas, $\dot{W}$ is the rate of work done by the system on the surroundings, and E_{system} is the total energy of the control volume system. The rate of work can be calculated from the FPA velocity, $\dot{x}$, the hot gas pressure, P_{gH}, and the hot gas piston area, A_g:

$$\dot{W} = A_g P_{gH} \dot{x} \quad (5)$$

Since the kinetic and gravitational potential energies of the hot gas are negligible, the total energy of the system is equal to the internal energy of the hot gas. This internal energy, assuming an ideal gas approximation, can be calculated from the gas temperature, T_g, the total mass of the gas, m_g, and the specific heat of the gas, c_v:

$$E_{system} = U = m_g c_v T_g \quad (6)$$

The mass of the gas can be also be expressed as the product of its density, ρ, the hot gas piston area, and FPA displacement:

$$m_g = \rho A_g x \quad (7)$$

Assuming ideal gas properties, the specific heat can be calculated from the gas constant, R and the specific heat ratio k, which are known properties of the gas:

$$c_v = \frac{R}{k-1} \quad (8)$$

Inserting Eq. 7 and 8 into Eq. 6 yields:

$$U = \frac{A_g x \rho R T_g}{k-1} = E_{system} \quad (9)$$

The ideal gas law can be written as:

$$P_{gH} = \rho R T_g \quad (10)$$

Substituting Eq. 10 into Eq. 9 yields:

$$E_{system} = \frac{A_g x P_{gH}}{k-1} \quad (11)$$

Differentiating Eq. 11 with respect to time:

$$\frac{d}{dt} E_{system} = \frac{A_g}{k-1} (\dot{x} P_{gH} + x \dot{P}_{gH}) \quad (12)$$

Since ideal gas properties are assumed, the enthalpy of the incoming hot gas can be determined from its temperature:

$$h_i = c_p T = k c_v T = \frac{kR}{k-1} T_{ad} \quad (13)$$

Substituting Eqs. 5, 12, and 13 into Eq. 4 yields:

$$\dot{P}_{gH} x + k P_{gH} \dot{x} = \dot{m}_i \frac{k R T_{ad}}{A_g} \quad (14)$$

Although no detailed analyses of hydrogen peroxide decomposition were found, past experimental results indicate a pure time delay of 37 msec between monopropellant injection and decomposition [6]. Thus, the mass flow rate of hot gas into the hot gas cylinder is approximated as the mass flow of monopropellant through the solenoid valve, $\dot{m}_{mono}$, shifted by a delay time, τ, as illustrated in Fig. 5.

$$\dot{m}_i(t) = \dot{m}_{mono}(t - \tau) \quad (15)$$

By combining Eq. 14 and 15 and reordering terms, an equation for the hot gas dynamics is produced:

$$\dot{P}_{gH}(t) = \frac{1}{x(t)} \left(\frac{\dot{m}_{mono}(t-\tau) k R T_{ad}}{A_g} - k P_{gH}(t) \dot{x}(t) \right) \quad (16)$$

Equation 4, and subsequently Eq. 16, assumes that the volume of the hot gas cylinder is equal to zero when the FPA position, x, is equal to zero. Since the volume of the hot gas cylinder is not zero when the FPHP begins a stroke, x can be defined as:

$$x = x_n + x_{clearance} \quad (17)$$

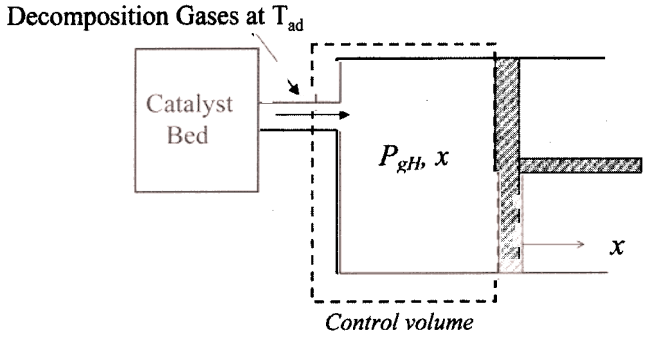

Fig. 4 Control Volume for Hot Gas Cylinder

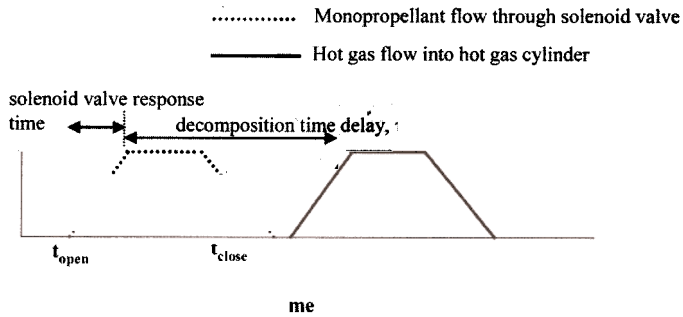

Fig. 5 Model of Monopropellant Flow Through Valve

where x_n is the FPA position which is equal to zero at the beginning of a stroke, and $x_{clearance}$ is the effective clearance length in the hot gas cylinder:

$$x_{clearance}=\frac{V_{clearance}}{A_g} \tag{18}$$

where $V_{clearance}$ is the volume of the hot gas cylinder at the beginning of each stroke. This extra volume includes any internal volume in the catalyst bed.

$$\dot{P}_{gH}(t)=\frac{1}{x_n(t)+x_{clearance}}\left(\frac{\dot{m}_{mono}(t-\tau)kRT_{ad}}{A_g}-kP_{gH}(t)\dot{x}_n(t)\right) \tag{19}$$

The dynamics of the mass flow of the monopropellant through the solenoid valve are estimated since there is no available data on specific valve dynamics other than the valve response time. The flow is modeled as a linear ramp to the steady state value over the valve response time as illustrated in Fig. 5. For small injection times, which are less than the decomposition time delay, the pressure drop across the solenoid valve is constant, and the steady state monopropellant flow is calculated from the valve flow equation as:

$$\dot{m}_{mono,ss}=\rho C_v\sqrt{\frac{\Delta P}{\gamma}} \tag{20}$$

where ρ is the density of the monopropellant, C_v is a geometry dependent valve constant, ΔP is the pressure drop across the valve and γ is the specific gravity of the monopropellant (ratio of density of monopropellant to density of water).

Equation 19 is used to model the high pressure gas during the initial portion of the expansion stroke. Once the hot gas piston crosses the exhaust port, it is assumed that the exhaust ports are large enough to vent the high gas pressure to atmospheric pressure instantaneously.

As the gas in the high pressure hot gas cylinder expands, the gas in the low pressure hot gas cylinder is compressed. During the initial portion of the stroke, while the exhaust port is still uncovered, the low pressure hot gas cylinder is still open to atmosphere so its pressure is assumed to be equal to atmospheric pressure. Once the low pressure hot gas piston passes the exhaust port, the low pressure side behaves as an air spring. Assuming the process is adiabatic, the pressure of the low pressure side is found from:

$$P_{gL}V^k=C \tag{21}$$

where V is the volume of the low pressure hot gas cylinder, k is the specific heat ratio, and C is a constant determined from the pressure and volume when the low pressure hot gas piston crosses the exhaust port. Since the pressure drops across the hydraulic check valves are small compared to the changes in gas pressures and the high pressure hydraulic force, P_{fL} and P_{fH} are assumed to be constant with P_{fL} set to the hydraulic reservoir pressure and P_{fH} equal to the maximum load pressure of the fluid in the accumulator. Although the load pressure would vary in real applications, if the FPHP can pump against the maximum load, it can pump against all loads. Since there are no side loads on the FPA, the friction is not dependent on the location of the FPA, as with a piston connected to a crankshaft, so F_{fric} is modeled as a constant.

4.2 Simulation Results. The first FPHP prototype was designed for a target power production of 2237 W (3 hp) at 6.9 $\times 10^6$ Pa (1000 psig) with an operating frequency (f) of 10 Hz. The power output (P) of the FPHP is calculated from:

$$P=2P_{fH}A_fL_{stroke}f \tag{22}$$

where P_{fH} is the hydraulic pressure, A_f is the area of the hydraulic piston, and L_{stroke} is the stroke length of the FPA.

Initial design simulations were performed, assuming 90% hydrogen peroxide and properties for off the shelf solenoid valves and catalyst beds, in order to determine a FPHP geometry which would provide the desired hydraulic power production. In order to maximize efficiency, the simulation varied the monopropellant injection time to find the minimum amount of injected monopropellant that would result in a successful stroke. The efficiency, ε, of the FPHP was then calculated as the ratio of work per stroke to the energy of the monopropellant injected (assuming an energy density, ED, of 1.2 MJ/kg for 90% hydrogen peroxide):

$$\varepsilon=\frac{\text{work extracted per stroke}}{\text{energy of fuel injected per stroke}}=\frac{P_{fH}A_fL_{stroke}}{ED} \tag{23}$$

The simulation parameters, which represent the monopropellant properties, valve characteristics, and FPHP geometry of the target prototype, are listed in Table 2. The monopropellant properties were taken from published data on hydrogen peroxide [1]. The FPHP geometry, mass properties, hydraulic pumping pressure, and reservoir pressure were taken from the design parameters of the prototype FPHP [13]. The dry friction was estimated from the forces required to manually push the FPA while assembling the pump. The steady state monopropellant flow through the solenoid valves was calculated from Eq. 20 using the measured C_v value of 0.015 (gal/min/psig$^{1/2}$) and monopropellant tank pressure of 3.4 $\times 10^6$ Pa (500 psig). The hot gas cylinder dead volume and the catalyst bed volume were calculated from the FPHP prototype data, and the decomposition time delay was estimated from literature on past hydrogen peroxide experiments [6].

The simulation, using the parameters in Table 2, resulted in an estimated efficiency of 21% for the initial prototype with a monopropellant injection time of 19 ms. The simulation results showing the FPA displacement and velocity and hot gas behavior over several cycles are shown in Figs. 6 and 7. Investigating the time duration of each stroke, it can be seen that a FPHP with these parameters is able to execute a full cycle, consisting of a right and

Table 2 Design Simulation Parameters

H_2O_2 concentration	90%
Gas Constant (R_{H2O2})	376 J/kgK
Specific Heat Ratio (k)	1.27
Adiabatic Decomposition Temperature (T_{ad})	1013 K
Steady State Monopropellant Mass Flow ($\dot{m}_{mono,ss}$)	0.025 kg/sec
Decomposition Time Delay (τ)	0.037 sec
Hydraulic Pressure in Accumulator (P_{fH})	6.9×10^6 Pa (1000 psig)
Hydraulic Reservoir Pressure (P_{fL})	2.8×10^5 Pa (40 psig)
Dry friction (F_{fric})	44 N
FPA Mass (m)	0.544 kg
Hot Gas Cylinder Diameter	0.0465 m (1.83 in)
Stroke Length	0.06 m (2.36 in)
Gas Cylinder to Hydraulic Cylinder Area Ratio (A_g/A_f)	6.5
Clearance Volume ($V_{clearance}$)	7.05×10^{-5} m^3 (4.3 in^3)

left stroke, in approximately 0.12 s. Thus, according to the simulation, the FPHP can operate near the target 10 Hz operating frequency.

5 Experimental FPHP

In order to demonstrate the feasibility of the design and the accuracy of the simulation, a prototype FPHP was designed and constructed following the parameters listed in Table 2 [13].

5.1 Hardware. The peripheral mechanical components of the FPHP experimental system, shown in Fig. 8, can be grouped into two main systems: the monopropellant system and the hydraulic system. The monopropellant system controls the flow of monopropellant, which is pressurized to 3.4×10^6 Pa (500 psig), into the catalyst beds. In order to simulate a maximum hydraulic load of 6.9×10^6 Pa (1000 psig), the FPHP pumps hydraulic fluid through a spring loaded relief valve between the accumulator and reservoir with a relief pressure of 6.9×10^6 Pa (1000 psig).

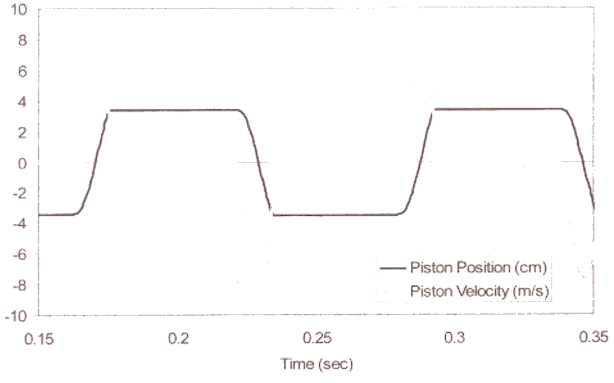

Fig. 6 Simulation Results for FPA Velocity and Position

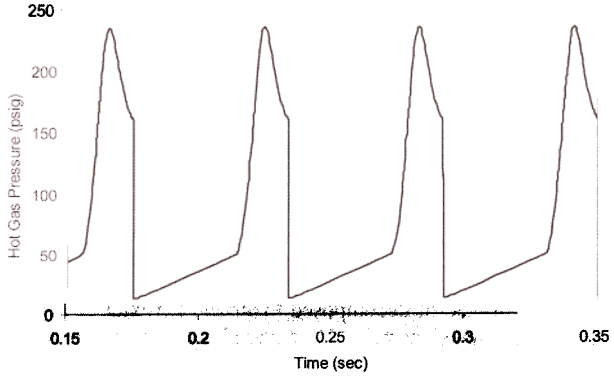

Fig. 7 Simulation Results for Hot Gas Pressure

5.2 Experimental Results. The FPHP was tested using a computer to control the time each solenoid valve was open. The best results were achieved by opening one solenoid valve for 500 ms and then waiting 4500 ms before pulsing the opposite valve. Figure 9 illustrates the recorded hot gas pressures in both hot gas cylinders over several cycles. Figure 10 shows a more detailed view of the hot gas pressures during one stroke of the FPHP. Even though the FPHP successfully pumped hydraulic fluid, several undesirable phenomenon were observed during testing, and the observed efficiency of 1.2% was significantly lower than expected. First, the FPA exhibited stiction-like behavior, with many of the strokes consisting of a series of small jerky motions instead of one

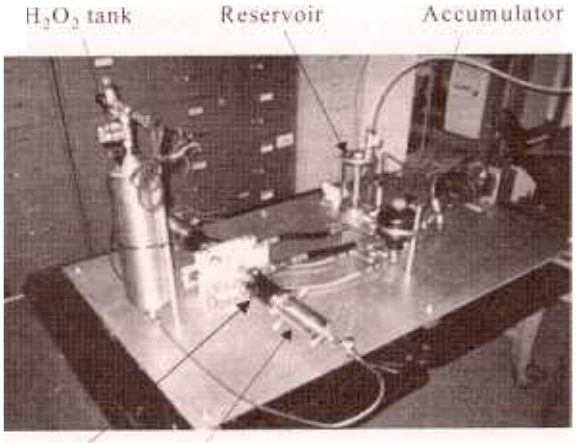

Fig. 8 Photo of the Experimental Power Source

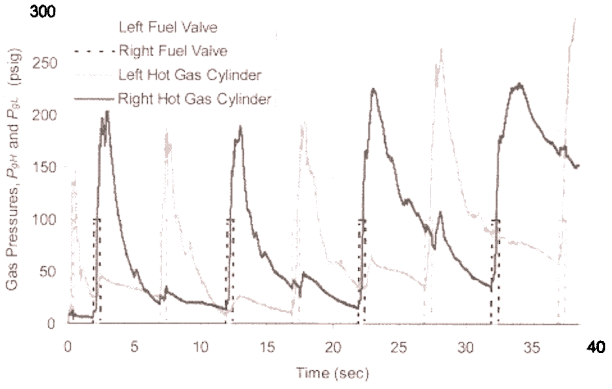

Fig. 9 Experimental Hot Gas Pressure with 500 ms Injection Time

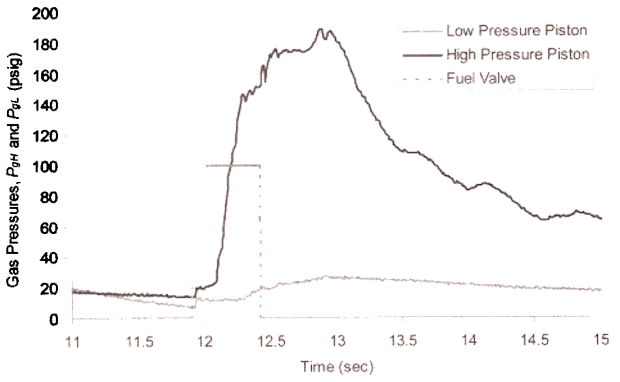

Fig. 10 Experimental Hot Gas Pressure Over Single Stroke

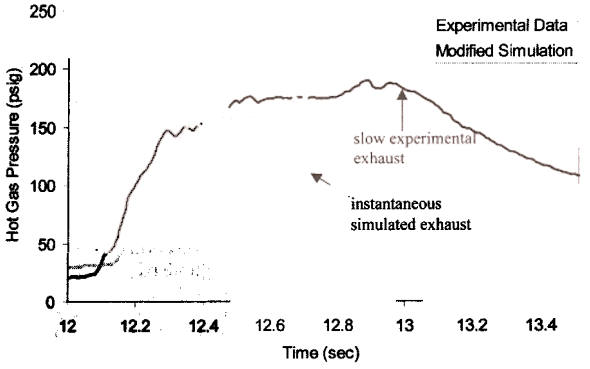

Fig. 12 Comparison of Experimental Data with Modified Simulation

smooth, continuous stroke. Second, most of the strokes resulted in a very slow exhaust of the hot gas, which was observed by a hissing sound. Third, over several cycles, the gas pressures on both sides of the FPHP gradually built up. Eventually, the excessive pressure on both sides prevented the FPHP from pumping at all, and the FPA remained stationary.

6 Discussion

During the simulation, short injection times of 19 ms produced quick pressure pulses on the order of tens of milliseconds as shown in Fig. 7, while much larger injection times of 500 ms were required on the actual system, producing much more gradual pressure rises and strokes lasting on the order of seconds as shown in Fig. 9. Upon careful evaluation of the experimental results and the prototype hardware, this discrepancy may be the result of poor delivery of the monopropellant from the solenoid valve to the catalyst bed. The required fittings to connect the solenoid valve and catalyst bed were rather large, creating a large amount of empty volume between the solenoid valve and catalyst bed. Figure 11 illustrates the interface between the solenoid valve and catalyst bed.

The monopropellant leaves the solenoid valve as fine mist, which would ideally directly enter the catalyst mesh. Instead, it is believed that the mist strikes the walls of the tubing and collects in the tube. The monopropellant then slowly drains into the silver catalyst mesh. Thus it is hypothesized that the actual flow rate of monopropellant into the catalyst bed is much lower than the mass flow rate of monopropellant from the solenoid valve.

In order to verify this hypothesis, several modifications were made to the original simulation. First, the dead volume in the hot gas cylinder was increased from 7.05×10^{-5} m^3 (4.3 in^3) to 1.15×10^{-4} m^3 (7.0 in^3) to account for the extra dead volume between the solenoid valve and the catalyst bed not accounted for in the initial design. Second, the steady state mass flow rate was changed from 0.025 to 0.001 kg/s to account for the hypothesis that the injected monopropellant collects in the space between the valve and catalyst, entering the catalyst at a much lower rate. The results of the modified simulation, plotted against the experimental data in Fig. 12, support the hypothesis that the monopropellant is in fact pooling between the valve and catalyst.

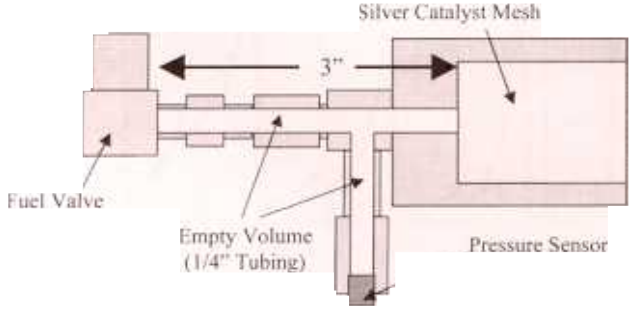

Fig. 11 Diagram of Solenoid Valve/Catalyst Interface

One important characteristic of both the experimental and simulated results in Fig. 12 is the smooth initial rise in pressure followed by oscillations in the pressure. This rise in pressure corresponds to the stage in the stroke when the FPA is stationary since the hot gas pressure is not high enough to overcome the high hydraulic force on the hydraulic piston. Looking at Eq. 19, which governs the hot gas pressure dynamics, the FPA velocity term, $\dot{x}_n$, is initially zero. Thus, the pressure change is positive since the term governed by the monopropellant injected, $\dot{m}_{mono}$, is always positive. Once the FPA begins to move, the velocity is no longer zero, and the negative FPA velocity term eventually dominates the positive monopropellant injection term since the actual rate of monopropellant entering the catalyst bed is so small. This causes the time derivative of the pressure to become negative. As the hot gas pressure drops, the hydraulic pressure slows the FPA. When the FPA is significantly slowed or sometimes stopped entirely, the positive monopropellant injection term of Eq. 19 again dominates, causing the time derivative of the pressure to become positive. As the hot gas pressure increases, it causes the FPA velocity to increase, resulting in a new drop in the hot gas pressure. This cycling of this process results in the pressure oscillations. These oscillations also account for the stiction-like behavior of the FPA, which was observed during testing as the pressure oscillations caused FPA velocity to cyclically increase and then drop to zero.

The collection of monopropellant between the valve and catalyst bed also accounts for the occasional increases in gas pressure long after the solenoid valves have been closed. A good example of this is the rise in pressure in the right gas chamber in Fig. 10 at 14.2 s. This pooling of monopropellant also creates a steady generation of hot gas on both sides of the FPHP as the collected monopropellant slowly drains into both catalyst beds. This gradual gas generation, along with the slow venting rates, accounts for the gradual pressure rise in both hot gas cylinders as seen in Fig. 9, which eventually prevented the FPA from moving.

One difference that remains between the modified simulation and the experimental result is the venting rate of the hot gas at the end of the stroke. As a result of the poor delivery of monopropellant to the catalyst bed, the hot gas pressures required to give the FPA enough momentum to fully uncover the exhaust port could not be achieved. During initial tests of the FPHP using compressed air instead of decomposed hydrogen peroxide to drive the piston, the exhaust port was uncovered and rapid exhaust was achieved, indicating that the improvement of the delivery of monopropellant to the catalyst bed will also solve the venting problem.

7 Conclusions

The simple and compact design of the FPHP allows inexpensive and robust power supply systems to be created. These systems, which offer a potential for improved energy and power density over electrical systems and the ability to produce intermittent power without idling in oxygen free environments, could have applications in a variety of mobile robotics applications. Although the experimental prototype of the monopropellant driven free piston hydraulic pump was not able to produce the target power output, it did demonstrate the feasibility of using a monopropellant to drive a piston engine and pump hydraulic fluid. The analysis of the experimental results also revealed that the integration of the solenoid valve and catalyst bed is essential to improve the delivery of the monopropellant to the catalyst bed. This knowledge can be applied to future versions of this type of system to greatly improve performance.

Acknowledgments

This paper was funded in part by ONR Grant N000-14-98-1-0669; NDSEG Fellowship; and NSF Fellowship.

References

[1] McCormick, J. C., 1967, "Hydrogen Peroxide Rocket Manual," FMC Corporation.

[2] Stokes, P. R., 1998, "Hydrogen Peroxide for Power and Propulsion," Presented at the London Science Museum, http://www.ee.surrey.ac.uk/SSC/H2O2CONF/Pstokes.htm.

[3] Dismukes, K. (curator), 2003, "Auxiliary Power Units," NASA Human Spaceflight Website, http://spaceflight.nasa.gov/shuttle/reference/shutref/orbiter/apu/

[4] Johnsen, E. G., and Corliss, and W. R., 1967, "Teleoperator and Human Augmentation," AEC-NASA Technology Survey, NASA Document SP-5047.

[5] Amendola, S. C., and Petillo, P. J., 2001, "Engine Cycle and Fuels for Same," United States Patent #6,250,078 B1.

[6] Barth, E. J., Gogola, M. A., Wehrmeyer, J. A., and Goldfarb, M., 2002, "The Design and Modeling of a Liquid-Propellant-Powered Actuator for Energetically Autonomous Robots," 2002 ASME International Mechanical Engineering Congress and Exposition Paper IMECE2002-DSC-32080.

[7] Beachley, N. H., and Fronczak, F. J., 1992, "Design of a Free-Piston Engine Pump," SAE paper 921740.

[8] Dalton, T. B., 1976, "Dual Pressure Hydraulic Pump," United States Patent #3,985,470.

[9] Heintz, R. P., 1978, "Free-Piston Engine-Pump Unit," United States Patent #4,087,205.

[10] Heintz, R. P., 1985, "Theory of Operation of a Free Piston Engine-Pump," SAE paper 859315.

[11] Li, L. J. and Beachley, N. H., 1988, "Design Feasibility of a Free Piston Internal Combustion Engine/Hydraulic Pump," SAE paper 880657.

[12] Tikkanen, S., and Vilenius, M., 1998, "On the Dynamic Characteristics of the Hydraulic Free Piston Engine," Second Tampere International Conference on Machine Automation.

[13] Raade, J. W., McGee, T. G., and Kazerooni, H., 2003, "Design, Construction, and Experimental Evaluation of a Monopropellant Powered Free Piston Hydraulic Pump," 2003 ASME International Mechanical Engineering Congress and Exposition Paper IMECE 2003-4260.